SUPPORTING INFORMATION

Electron Exchange Capacity of Pyrogenic Dissolved Organic Matter (pyDOM): Complementarity of Square-Wave Voltammetry in DMSO and Mediated Chronoamperometry in Water

Han Cao[1], Ania S. Pavitt[2], Jeffrey M. Hudson[2], Paul G. Tratnyek[2]*, Wenqing Xu[1]*

[1] Department of Civil and Environmental Engineering, Villanova University, Villanova, Pennsylvania 19085, United States

[2] OHSU/PSU School of Public Health, Oregon Health & Science University, 3181 SW Sam Jackson Park Road, Portland, OR 97239, United States

*Corresponding authors:

Email: tratnyek@ohsu.edu, Phone: 503-346-3431

Email: wenqing.xu@villanova.edu, Phone: 610-519-8549

Supporting Information File for Environmental Science: Processes & Impacts

Contents: 38 pages, 13 Figures, 11 Tables, 5 Texts, and 19 References

Table of Contents

Table S1. Samples of natural organic matter (NOM) used in this study.

NOM [a]	Cat. No.	Elemental composition (wt%) [b]				Atomic ratio (mol/mol)		Class [c]
		C	H	O	N	H/C	O/C	
ESHA	1S102H	58.13	3.68	34.08	4.14	0.76	0.44	T
LHA	1S104H	63.81	3.70	31.27	1.23	0.70	0.37	T
PPFA	2S103F	51.31	3.53	43.32	2.34	0.83	0.63	T
PPHA	1S103H	56.37	3.82	37.34	3.69	0.81	0.50	T
SRFA	2S101F	52.34	4.36	42.98	0.67	0.99	0.62	A
SRNOM	1R101N	52.47	4.19	42.69	1.10	0.95	0.61	A

[a] All NOMs are acquired from International Humic Substance Society (IHSS). The abbreviations are ESHA: Elliott Soil humic acid; LHA: Leonardite humic acid; PPHA: Pahokee Peat fulvic acid; PPFA: Pahokee Peat humic acid; SRFA: Suwannee River fulvic acid; SRNOM: Suwannee River natural organic matter.

[b] Elemental composition were obtained from IHSS website: https://humic-substances.org/elemental-compositions-and-stable-isotopic-ratios-of-ihss-samples/.

[c] Class refers to terrestrial (T) or aquatic (A) NOM.

Table S2. Material characterization of the chars used in this study.

Char [a,b]	Elemental composition (wt%)					Atomic ratio (mol/mol)		Surface Area ($m^2 \cdot g^{-1}$) [c]	pH [d]
	C	H	O	N	Ash	H/C	O/C		
W300	50.1	3.8	38.4	< 0.5	2.2	0.91	0.57	260.0	3.02
W400	64.1	3.4	25.4	0.6	1.5	0.64	0.30	496.5	3.45
W500	75.8	3.0	14.8	0.5	2.9	0.47	0.15	574.8	8.91
W600	81.2	2.1	10.3	0.6	2.9	0.31	0.10	528.8	9.13
W700	86.6	2.3	5.5	0.5	3.2	0.32	0.05	725.4	10.35
G300	40.0	5.5	36.4	0.7	9.3	1.65	0.68	282.5	4.64
G400	59.9	4.2	20.9	0.8	10.4	0.84	0.26	443.7	7.57
G500	65.9	3.0	17.3	0.8	9.6	0.55	0.20	497.7	9.23
G600	74.6	3.4	6.4	0.7	11.0	0.55	0.06	595.6	9.48
G700	76.3	2.1	6.8	0.6	11.7	0.33	0.07	547.7	9.96

[a] W or G represents wood (*Quercus*) or grass (*Panicum vigartum*) feedstock, respectively, whereas the number corresponds to pyrolysis temperature.
[b] Pyrolyzed under oxygen-limited conditions in a muffle furnace for 2 h.
[c] Characterized by BET N_2 sorption.
[d] Determined in a homogeneous suspension by equilibrating the respective char with DI water at a solid-to-liquid ratio of 100 $g_{char} \cdot L^{-1}$ following American Society for Testing and Materials (ASTM) D3838-05 (Standard Test Method for pH of Activated Carbon; 2017).

Table S3. Non-purgeable organic carbon (NPOC) concentrations, specific UV absorbance at 254 nm ($SUVA_{254}$), and the ratio of absorbances at 254 and 365 nm ($E_2 \cdot E_3^{-1}$) from raw pyDOM and NOM samples.

Sample	NPOC [a,b] ($mg_C \cdot L^{-1}$)	$SUVA_{254}$ [a] ($L \cdot mg_C^{-1} \cdot m^{-1}$)	$E_2 \cdot E_3^{-1}$ [a]
$pyDOM_{W300}$	113.3±1.4	4.7±0.0	5.5±0.1
$pyDOM_{W400}$	59.3±7.3	2.2±0.1	9.1±0.1
$pyDOM_{W500}$	30.0±1.8	5.3±0.0	8.5±0.0
$pyDOM_{W600}$	34.5±6.3	6.2±0.0	13.4±0.6
$pyDOM_{W700}$	5.8±1.2 [c]	11.0±0.1	6.1±0.5
$pyDOM_{G300}$	97.1±9.7	2.6±0.0	5.9±0.1
$pyDOM_{G400}$	30.2±0.3	2.1±0.0	6.9±0.6
$pyDOM_{G500}$	24.2±1.1	2.6±0.4	9.2±1.1
$pyDOM_{G600}$	26.7±1.2	4.2±0.2	12.1±0.6
$pyDOM_{G700}$	12.1±0.8 [c]	3.6±0.1	6.7±0.7
ESHA	220.4±3.6	4.8±0.0	3.1±0.0
LHA	98.3±6.7	8.3±0.0	3.2±0.0
PPFA	5218.9±78.1	8.2±0.0	4.2±0.0
PPHA	690.1±14.2	9.3±0.0	3.1±0.0
SRFA	5039.7±6.8	6.0±0.0	4.3±0.0
SRNOM	4422.1±18.0	1.0±0.0	5.1±0.0

[a] ±values are the standard errors from duplicate measurements on independently prepared samples.
[b] NPOC values are not representative values in SWV or MCA experiments.
[c] The extracted NPOC of $pyDOM_{W700}$ and $pyDOM_{G700}$ from 160 $g_{char} \cdot L^{-1}$ are 33.04±1.71 and 134.86±17.12 $mg_C \cdot L^{-1}$, respectively.

Table S4. Total concentrations of manganese (Mn) and iron (Fe), and the estimated contribution to the overall electron exchange capacity (EEC) in pyDOM and NOM.

Sample	Metal concentration ($\mu g \cdot L^{-1}$) [a]		EEC of metal ($\mu mol_{e-} \cdot L^{-1}$) [b]		Metal contribution to EEC_{pyDOM} (%) [c,d,e]	
	Mn	Fe	Mn^{4+}/Mn^{2+}	Fe^{3+}/Fe^{2+}	Mn^{4+}/Mn^{2+}	Fe^{3+}/Fe^{2+}
$pyDOM_{W300}$	180.36	<LoQ	6.56	--	3.67	--
$pyDOM_{W400}$	252.25	<LoQ	9.17	--	5.97	--
$pyDOM_{W500}$	136.51	<LoQ	4.96	--	4.20	--
$pyDOM_{W600}$	248.45	<LoQ	9.03	--	7.60	--
$pyDOM_{W700}$	1379.67	<LoQ	50.17	--	426.32	--
$pyDOM_{G300}$	662.82	<LoQ	24.10	--	12.05	--
$pyDOM_{G400}$	1105.64	<LoQ	40.20	--	39.01	--
$pyDOM_{G500}$	1266.93	<LoQ	46.07	--	45.35	--
$pyDOM_{G600}$	1605.19	<LoQ	58.37	--	47.03	--
$pyDOM_{G700}$	965.21	<LoQ	35.10	--	81.35	--
ESHA	<LoQ	<LoQ	--	--	--	--
LHA	<LoQ	331.57	--	5.92	--	0.53
PPFA	<LoQ	3005.18	--	53.67	--	0.27
PPHA	<LoQ	1914.82	--	34.19	--	1.26
SRFA	20.80	3691.28	0.76	65.92	0.0027	0.23
SRNOM	<LoQ	169.45	--	3.03	--	0.43

[a] Metal concentration was measured by ICP-MS; the limit of quantification (LoQ) was 0.03 $\mu g \cdot L^{-1}$ and 0.1 $\mu g \cdot L^{-1}$ for Mn and Fe, respectively.

[b] EEC contributed by Mn and Fe were calculated based on the assumption that 2 mole e^- was transferred by per mole Mn (Mn^{4+}/Mn^{2+}), and 1 mole e^- was transferred by per mole Fe (Fe^{3+}/Fe^{2+}).

[c] $EEC_{pyDOM} = EDC_{pyDOM} + EAC_{pyDOM}$.

[d] The metal contribution was calculated by dividing the EEC of pyDOM or NOM (converted from the unit of $\mu mol_{e-} \cdot g_C^{-1}$ to $\mu mol_{e-} \cdot L^{-1}$ by multiplying the NPOC concentration in $mg_C \cdot L^{-1}$) by EEC of metal.

[e] The metal contribution is for reference purpose, while the actual valence states of the metals are unknown.

Text S1. Quantification and calibration details of SWV method.

The calibration method for SWV analysis was validated with two well-studied model quinones as redox standards (RS), detail of which is recorded in **Text S3**. Peak area (PA) for the SWV method is defined by equation (eq) S1:

$$\mathbf{PA\ (A \cdot V)\ =\ \int_{E1}^{E2} I \bullet dE} \qquad \text{(S1)}$$

where E_1 and E_2 are the start and end potentials for the peak, respectively. The SWV output results of PA are in the units of A·V. Anodic peaks were used to obtain PA_{SWVa} and cathodic peaks were used to obtain PA_{SWVc}.

The resulting values of PA were divided by the scan rate (v; $V \cdot s^{-1}$) with eq S2 to obtain charge transferred (Q) in Coulombs (C), which could then be divided by the Faraday constant (F = 96,485 $C \cdot mol_{e-}^{-1}$) to give Q in moles of electrons with eq S3.

$$\mathbf{Q\ (in\ C)\ =\ PA/v} \qquad \text{(S2)}$$

$$\mathbf{Q\ (moles\ of\ e^{-})\ =\ Q\ (in\ C)/F} \qquad \text{(S3)}$$

From here, Q can be normalized to the mass of organic carbon (NPOC; g_C) present in the sample, providing a method of EEC calculation we hereby refer to as the Faraday method, the values of which were provided in **Table S5**. This method has been used in a previous study to obtain EEC values of pyrogenic carbon samples, where cyclic voltammetry was performed on immobilized pyrogenic carbon samples bound to the surface of a small working electrode by nafion.[1]

However, most data obtained by voltammetry do not represent complete reaction between the electrode and bulk analyte in the cell. This inefficiency is determined by operational factors that usually are best corrected using an experimentally determined response factor or calibration curve obtained with model compounds that have relatively ideal electrode response. To enable comparison between SWV and MCA, we used calibration with both methods.

Calibration curves were obtained by SWV with varying concentrations of well-characterized electron-transfer mediators (ETMs), using the same electrochemical cell and methods used for the analyte measurements (detailed in the methods section). Previous work with chronoamperometry in microfluidic cells used ascorbic acid for MEO, and AQDS for MER.[2] For SWV, we used only AQDS, as AQDS displays suitable electrochemically reversible behavior and is commonly used as an analog for redox-active moieties in NOM.

For the dependent variable (y) in the calibration curve (**Figure S1**), the directly measured electrode response (i.e., PA) was used. While AQDS in SWV exhibited multiple peaks during both the anodic and cathodic scans, we decided to use only the largest, main peak for calculation of PA in our regression analysis. For the independent variable (x), the concentration of the ETM was expressed as X ($mol_{e^-} \cdot L^{-1}$) and calculated using the experimentally prepared molar concentration of ETM multiplied by the theoretical stoichiometry of the AQDS redox couple (i.e., n = 2).

The resulting regression equations (**Figure S1**) were used to back-calculate the X values of the experimental samples with their PA values. Subsequently, the electron donating or accepting capacities for SWV (EDC_{SWV} or EAC_{SWV}, respectively) for each experimental sample was obtained from eq S4:

$$\mathbf{EDC_{SWV}\ or\ EAC_{SWV}\left(mol_{e^-} \cdot g_C^{-1}\right) = X\left(mol_{e^-} \cdot L^{-1}\right)/NPOC\left(g_C \cdot L^{-1}\right)} \quad \text{(S4)}$$

where the NPOC is determined from the sample analyzed in the electrochemical cell. The resulting values of PA, Q, and EECs for all samples are reported in **Tables S5 and S6**. We also reported their sum (i.e., EDC_{SWV} + EAC_{SWV}), which we labelled as EEC_{SWV}, to be consistent with nomenclature developed for use with the MCA method. However, we note that EEC_{SWV} may not be fully analogous to EEC_{MCA}, as discussed in the MT.

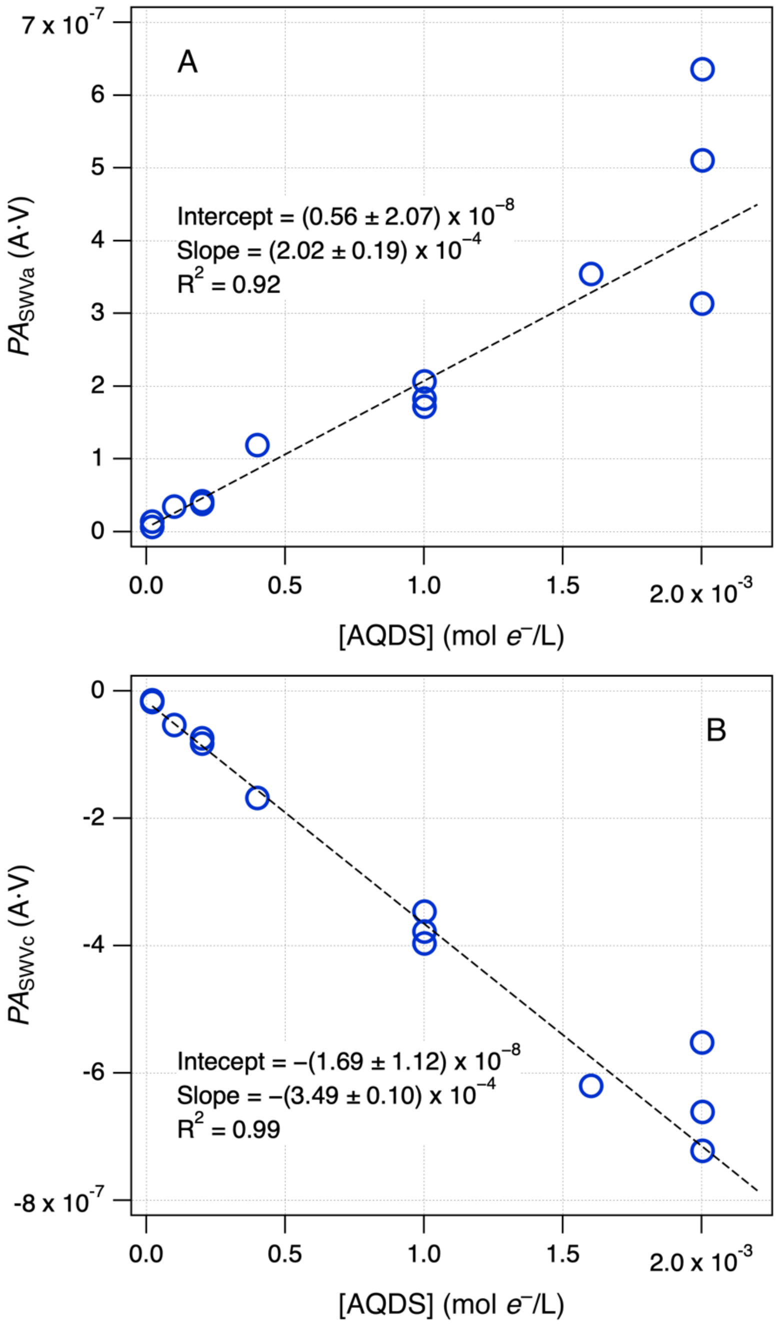

Figure S1. Calibration curves applied to convert square-wave voltammetry (SWV) peak areas (PA_{SWVa} or PA_{SWVc}) to charge transferred (Q_{ox} or Q_{red}) in $mol_{e-}\cdot L^{-1}$ in electron exchange capacity (EEC) calculations.

Table S5. Non-purgeable organic carbon (NPOC), peak area (PA), charge transferred (Q) and EECs obtained by SWVa and SWVc for pyDOM and NOM samples via the Faraday method.

Sample	NPOC [a]	PA_{SWVa} [b]	PA_{SWVc} [b]	Q_{ox} [c]	Q_{red} [c]	$EDC_{Faraday}$ ($mmol_{e^-}\cdot g_C^{-1}$) [d]	$EAC_{Faraday}$ ($mmol_{e^-}\cdot g_C^{-1}$) [d]	$EEC_{Faraday}$ ($mmol_{e^-}\cdot g_C^{-1}$) [d]
$pyDOM_{W300}$	5.72E−05	2.18E−07	4.14E−07	8.72E−06	1.66E−05	1.60E−03	3.03E−03	4.63E−03
$pyDOM_{W400}$	3.02E−05	1.25E−07	3.66E−07	4.99E−06	1.47E−05	1.74E−03	5.12E−03	6.87E−03
$pyDOM_{W500}$	1.56E−05	1.95E−07	1.16E−07	7.81E−06	4.65E−06	5.39E−03	3.21E−03	8.60E−03
$pyDOM_{W600}$	1.78E−05	1.06E−07	1.49E−07	4.25E−06	5.96E−06	2.55E−03	3.58E−03	6.14E−03
$pyDOM_{W700}$	3.45E−06	2.80E−07	1.11E−07	1.12E−05	4.45E−06	4.03E−02	1.60E−02	5.64E−02
$pyDOM_{G300}$	4.91E−05	1.48E−07	3.77E−07	5.92E−06	1.51E−05	1.26E−03	3.22E−03	4.49E−03
$pyDOM_{G400}$	1.57E−05	1.91E−07	2.20E−07	7.63E−06	8.80E−06	5.24E−03	6.05E−03	1.13E−02
$pyDOM_{G500}$	1.27E−05	1.39E−07	1.38E−07	5.56E−06	5.53E−06	4.77E−03	4.74E−03	9.51E−03
$pyDOM_{G600}$	1.39E−05	1.51E−07	1.61E−07	6.03E−06	6.43E−06	4.67E−03	4.99E−03	9.66E−03
$pyDOM_{G700}$	6.61E−06	7.55E−08	1.57E−07	3.02E−06	6.28E−06	5.19E−03	1.08E−02	1.60E−02
ESHA	1.13E−04	2.12E−07	2.28E−07	8.47E−06	9.12E−06	7.97E−04	8.58E−04	1.65E−03
LHA	5.20E−05	8.62E−08	4.11E−07	3.45E−06	1.64E−05	7.27E−04	3.47E−03	4.19E−03
PPFA	2.62E−03	5.38E−07	9.75E−07	2.15E−05	3.90E−05	8.55E−05	1.55E−04	2.40E−04
PPHA	3.48E−04	1.52E−07	5.25E−07	6.08E−06	2.10E−05	1.83E−04	6.31E−04	8.13E−04
SRFA	2.53E−03	4.71E−07	6.31E−07	1.89E−05	2.52E−05	7.75E−05	1.04E−04	1.81E−04
SRNOM	2.22E−03	6.20E−07	9.17E−07	2.48E−05	3.67E−05	1.16E−04	1.72E−04	2.88E−04

[a] NPOC in the electrochemical cell (g).
[b] PA is main peak areas (inner area only, excluding one outermost peak on each side) (A·V) for both anodic and cathodic scans.
[c] Q is charge (C, A·s) measured for each sample during anodic (ox) and cathodic (red) scans.
[d] All values are obtained from the integrated area of the main peaks of SWV and divided by the scan rate and Faraday constant.

Table S6. Non-purgeable organic carbon (NPOC), peak area (PA), and EECs obtained by SWVa and SWVc for pyDOM and NOM samples using the calibration method.

Sample	NPOC [a]	PA_{SWVa} [b]	PA_{SWVc} [b]	EDC_{SWV} ($mmol_{e^-} \cdot g_C^{-1}$) [c]	EAC_{SWV} ($mmol_{e^-} \cdot g_C^{-1}$) [c]	EEC_{SWV} ($mmol_{e^-} \cdot g_C^{-1}$) [c]
$pyDOM_{W300}$	1.04E−02	2.18E−07	4.14E−07	1.02E+02	1.11E+02	2.13E+02
$pyDOM_{W400}$	5.49E−03	1.25E−07	3.66E−07	1.10E+02	1.86E+02	2.95E+02
$pyDOM_{W500}$	2.83E−03	1.95E−07	1.16E−07	3.44E+02	1.04E+02	4.49E+02
$pyDOM_{W600}$	3.24E−03	1.06E−07	1.49E−07	1.59E+02	1.21E+02	2.80E+02
$pyDOM_{W700}$	6.28E−04	2.80E−07	1.11E−07	2.60E+03	5.17E+02	3.11E+03
$pyDOM_{G300}$	8.94E−03	1.48E−07	3.77E−07	7.99E+01	1.17E+02	1.97E+02
$pyDOM_{G400}$	2.85E−03	1.91E−07	2.20E−07	3.34E+02	2.12E+02	5.47E+02
$pyDOM_{G500}$	2.30E−03	1.39E−07	1.38E−07	3.01E+02	1.58E+02	4.59E+02
$pyDOM_{G600}$	2.54E−03	1.51E−07	1.61E−07	2.96E+02	1.70E+02	4.65E+02
$pyDOM_{G700}$	1.20E−03	7.55E−08	1.57E−07	3.16E+02	3.66E+02	6.82E+02
ESHA	2.06E−02	2.12E−07	2.28E−07	5.10E+01	3.02E+01	8.12E+01
LHA	9.45E−03	8.62E−08	4.11E−07	4.47E+01	1.26E+02	1.71E+02
PPFA	4.76E−01	5.38E−07	9.75E−07	5.56E+00	5.79E+00	1.13E+01
PPHA	6.33E−02	1.52E−07	5.25E−07	1.16E+01	2.32E+01	3.48E+01
SRFA	4.59E−01	4.71E−07	6.31E−07	5.04E+00	3.84E+00	8.88E+00
SRNOM	4.03E−01	6.20E−07	9.17E−07	7.57E+00	6.42E+00	1.40E+01

[a] NPOC in the electrochemical cell ($g \cdot L^{-1}$).
[b] PA is main peak areas (inner area only, excluding one outermost peak on each side) ($A \cdot V$) for both anodic and cathodic scans.
[c] All the values are obtained from main peaks of SWV then calibrated with 9,10-Anthraquinone-2,6-disulfonic acid disodium salt (AQDS) as a redox standard.

Text S2. Quantification and calibration details of MCA method.

The calibration method for MCA analysis was also validated with two well-studied model quinones as redox standards (RS), the details of which is recorded in **Text S3**. Peak Area (PA) for the MCA method is defined by eq S5:

$$\mathbf{PA\ (A \cdot s)\ =\ \int_{t1}^{t2} I\, dt} \tag{S5}$$

where I is the current (A) response, t is time (s), t_1 and t_2 are the start and end times of the identified peak, respectively. The MCA output results of PA that are in the units of A·s. Peaks from mediated electrochemical oxidation (MEO) were used to obtain PA_{MEO}, while those from mediated electrochemical reduction (MER) were used to obtain PA_{MER}.

The calibration curve used to calculate the electron transfer (Q) was obtained by adding known concentrations of well-behaved RS and measuring the electrode response with the same electrochemical cell that used for the analyte measurements (detailed in the methods section). We selected the same RS for calibration as previous studies using MCA with FIA: ascorbate for EDC and AQDS for EAC.[2]

Assuming both RS fully react with ideal stoichiometry (i.e., $EDC_{ascorbate}$= 2.00 $mol_{e-} \cdot mol_{ascorbate}^{-1}$; EAC_{AQDS} = 2.00 $mol_{e-} \cdot mol_{AQDS}^{-1}$), the calibration curves for EDC and EAC (panels C and D in **Figure S2**) were constructed by plotting PA vs. Q (in μmol_{e-}), which was calculated with eq S6.

$$\mathbf{Q\ (\mu mol_{e-})\ =\ 2 \cdot \frac{\mu mol_{e-}}{\mu mol_{RS}} \cdot C_{RS} \cdot V_{RS}} \tag{S6}$$

where C_{RS} is in $\mu mol \cdot L^{-1}$; V_{RS} is the injected volume (L) of the stock solution of RS. The calibration equation was then obtained by linear regression on the data in **Figure S2**.

Next, the calibration equations of MEO (**Figure S2C**) and MER (**Figure S2D**) were applied to PA_{MEO} and PA_{MER} of each injected sample to obtain their Q_{MEO} and Q_{MER}. Finally, EDC or EAC ($mmol_{e-} \cdot g_C^{-1}$) were obtained by normalizing Q (in μmol_{e-}) with the amount of NPOC ($mg_C \cdot L^{-1}$) injected following eq S7:

$$\mathbf{EDC\ or\ EAC\ =\ Q/(NPOC \cdot V)} \tag{S7}$$

where NPOC is in $mg_C \cdot L^{-1}$, V is the injection volume (L) of the sample. The resulting values of PA, Q, and EECs for all samples are reported in **Table S7**.

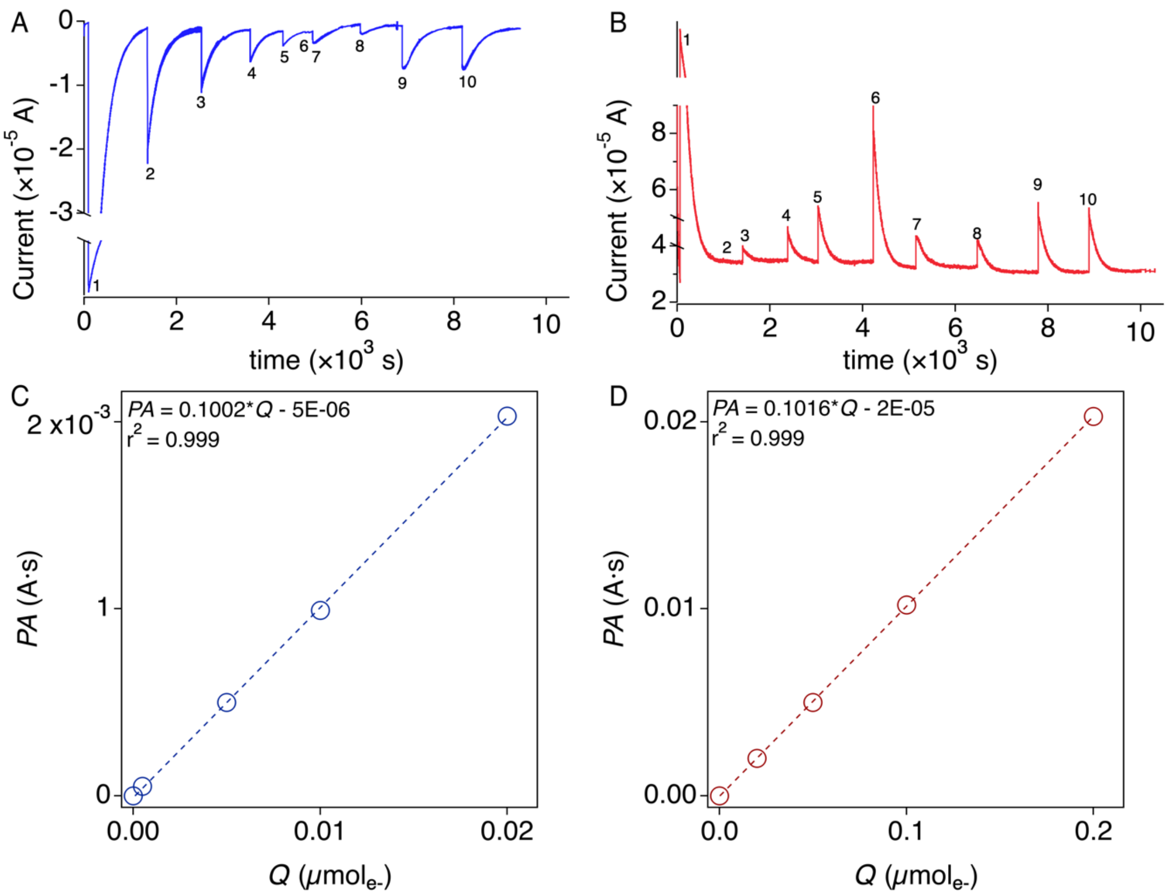

Figure S2. Example peaks for (A) MEO and (B) MER analysis for redox standards (RS), pyDOM$_{W300}$, and Leonardite humic acid (LHA). The electrochemical cell was maintained at E_H = −0.49 and +0.61 V vs. standard hydrogen electrode (SHE) at pH 7 (0.1M KCl, 0.1M phosphate buffer). Peak 1 of panels (A) and (B) are the injections of mediator (ABTS for MEO and DQ for MER); peaks 2-6 are serial injections of ascorbate (0 – 0.02 µmol$_{e-}$) or AQDS (0 – 0.2 µmol$_{e-}$); peaks 7 and 8 are duplicate injections of pyDOM$_{W300}$; peaks 9 and 10 are duplicate injections of LHA. Each injection was conducted after the background current returned to plateau. Panel (C) is electron donating capacity (EDC) calibration curve applied in mediated electrochemical oxidation (MEO) analysis, and panel (D) is electron accepting capacity (EAC) calibration curve applied in mediated electrochemical reduction (MER) analysis. Each mole of redox standard (ascorbate or AQDS) was assumed to transfer 2 moles of electron (i.e., $EDC_{ascorbate}$ = 2.00 mol_{e-} $mol_{ascorbate}^{-1}$, EAC_{AQDS} = 2.00 mol_{e-} mol_{AQDS}^{-1}).[2]

Text S3. Validation of SWV and MCA method using model quinones.

Two model quinones, 5-Hydroxy-1,4-naphthoquinone (juglone) and 1,2-Naphthoquinone-4-sulfonic acid (o-NQS), were used as RS to verify the accuracy of the SWV and MCA methods. For the SWV method, the two RS were dissolved in DMSO to obtain concentrated stock solutions, from which 0.5 ml of the analyte was added into an electrochemical cell consisting of 5 ml 0.1M TBAFP dissolved in DMSO to obtain final concentrations within the cell of approximately 1.5 mM. The SWV measurements were made using the same protocols as for the pyDOM or NOM samples, described in method section. For both RS, all of the major SWV peaks (typically 2, **Figure S12A and 12D**) were integrated and summed to obtain total area (**Figure S13**), but we only report data for the largest "main" peak to be consistent with the calibration obtained using AQDS (**Text S1** and **Figure S1**). The main PAs obtained by integration with Igor were compared to those obtained using other software (e.g., Origin Lab), and the results were similar. Finally, the main PAs from anodic and cathodic SWV data were converted to values of EDC and EAC, respectively, using the calibration curved obtained with AQDS (as described in **Text S1**).

For validation of the MCA method, the two RS were prepared with the same experimental conditions used for the measurements on pyDOM or NOM samples, described in method section. RS solutions were prepared in 10 mM phosphate buffer solution (PBS; pH 7) then passed through 0.45 μm PTFE filters. NPOC was measured in a TOC analyzer and MCA measurements were performed at fixed potentials of +0.61 V and −0.49 V (vs. SHE) for MEO and MER, respectively. The peaks obtained with the RS were integrated to obtain PAs, and converted to EECs as described in **Text S2**.

The EDCs and EACs obtained for juglone and o-NQS are given in **Tables S9 and S10** for SWV and MCA, respectively. In all cases, the measured values were slightly higher than the theoretical value of 2.0, with the medium difference being about 1.5-fold. This modest deviation from ideal response could easily result from inaccuracy in the calibration curves, due to operational factors with ad hoc effects on electrode response. In MCA analysis, the NPOC normalized EAC results of two RS showed significantly higher values than pyDOM or NOM samples. Once normalized to the unit of $mmol_{e-} \cdot mmol_{RS}^{-1}$, they fall in a reasonable range and match the expected stoichiometry. Both juglone and o-NQS have negligible EDC compared to their EAC, due to both quinones being in their oxidized states at the onset of experiments and the limitation of MCA operating at fixed potentials in comparison to the large redox range and reversible nature of SWV experiments. Both SWV and MCA showed higher EAC in juglone than o-NQS, indicating that juglone is more redox active in both methods. While the exact reason behind this difference is unclear, one possibility could be the steric effects among different quinones and their interactions with the electrode surface led to the elevated redox reactivity observed here and in other studies.[3,4] As with the pyDOM and NOM data, EEC_{SWV}

values obtained with the model quinones are nearly twice as those obtained by EEC_{MCA}. The significance of this comparison is discussed in the main text.

Table S7. Non-purgeable organic carbon (NPOC), peak area (PA), charge transferred (Q) and EECs obtained by MEO and MER for pyDOM and NOM samples.

Sample	NPOC [a]	PA_{MEO} [b,d]	PA_{MER} [b,d]	Q_{MEO} [c,d]	Q_{MER} [c,d]	EDC_{MCA} ($mmol_{e^-}\cdot g_C^{-1}$) [d]	EAC_{MCA} ($mmol_{e^-}\cdot g_C^{-1}$) [d]	EEC_{MCA} ($mmol_{e^-}\cdot g_C^{-1}$) [d]
$pyDOM_{W300}$	1.13E−05	3.84E−04 ±9.23E−05	1.91E−03 ±1.11E−04	3.89E−06 ±9.22E−04	1.90E−05 ±1.09E−06	0.34±0.08	1.68±0.10	2.02±0.18
$pyDOM_{W400}$	5.93E−06	3.19E−04 ±7.62E−05	1.55E−03 ±3.83E−04	3.23E−06 ±7.61E−07	1.55E−05 ±3.77E−06	0.54±0.13	2.61±0.63	3.15±0.76
$pyDOM_{W500}$	3.00E−06	2.05E−04 ±2.72E−05	1.67E−03 ±1.27E−04	2.10E−06 ±2.72E−07	1.66E−05 ±1.25E−06	0.70±0.09	5.52±0.42	6.22±0.51
$pyDOM_{W600}$	3.45E−06	5.25E−05 ±1.60E−05	1.46E−03 ±1.22E−04	5.73E−07 ±1.59E−07	1.45E−05 ±1.20E−06	0.17±0.05	4.21±0.35	4.38±0.40
$pyDOM_{W700}$	3.30E−06	8.98E−05 ±1.39E−05	4.70E−04 ±1.70E−05	9.46E−07 ±1.38E−07	4.83E−06 ±1.67E−07	0.29±0.04	1.46±0.05	1.75±0.09
$pyDOM_{G300}$	9.71E−06	4.43E−04 ±1.12E−04	1.54E−03 ±2.23E−04	4.48E−06 ±1.12E−06	1.54E−05 ±2.19E−06	0.46±0.12	1.58±0.23	2.04±0.35
$pyDOM_{G400}$	3.02E−06	2.15E−04 ±2.05E−06	8.22E−04 ±4.36E−05	2.20E−06 ±2.05E−08	8.29E−06 ±4.29E−07	0.73±0.01	2.75±0.14	3.48±0.15
$pyDOM_{G500}$	2.42E−06	7.41E−05 ±2.05E−05	1.14E−03 ±4.88E−05	7.89E−07 ±2.05E−07	1.14E−05 ±4.80E−07	0.33±0.08	4.70±0.20	5.03±0.28
$pyDOM_{G600}$	2.67E−06	7.76E−05 ±1.29E−05	1.32E−03 ±9.76E−05	8.24E−07 ±1.29E−07	1.32E−05 ±9.60E−07	0.31±0.05	4.93±0.36	5.24±0.41
$pyDOM_{G700}$	1.35E−05	2.37E−04 ±7.23E−05	2.22E−03 ±9.62E−05	2.42E−06 ±7.22E−07	2.20E−05 ±9.47E−07	0.18±0.05	1.63±0.07	1.81±0.12
ESHA	2.20E−05	2.30E−03 ±2.81E−04	4.70E−03 ±1.01E−03	2.30E−05 ±2.80E−06	4.64E−05 ±9.97E−06	1.04±0.13	2.11±0.45	3.15±0.58
LHA	9.83E−06	2.37E−03 ±1.63E−05	3.49E−03 ±6.49E−04	2.37E−05 ±1.62E−07	3.45E−05 ±6.39E−06	2.41±0.02	3.51±0.65	5.92±0.67

PPFA	5.22E−04	1.08E−01 ±6.36E−03	6.98E−02 ±8.41E−03	1.07E−03 ±6.35E−05	6.87E−04 ±8.28E−05	2.06±0.12	1.32±0.16	3.38±0.28
PPHA	6.90E−05	1.16E−02 ±2.73E−03	1.44E−02 ±1.41E−04	1.16E−04 ±2.73E−05	1.42E−04 ±1.39E−06	1.69±0.40	2.06±0.02	3.75±0.42
SRFA	5.04E−04	2.45E−01 ±2.69E−03	3.71E−02 ±9.90E−05	2.44E−03 ±2.68E−05	3.65E−04 ±9.74E−07	4.84±0.05	0.72±0.00	5.56±0.05
SRNOM	4.42E−04	1.14E−01 ±8.06E−04	4.86E−02 ±5.32E−03	1.13E−03 ±8.04E−06	4.78E−04 ±5.23E−05	2.56±0.02	1.08±0.12	3.64±0.14

[a] NPOC in the electrochemical cell (g).
[b] PA (A·s) is peak areas derived from integration of each peak generated from sample injections.
[c] Q ($mmol_{e-}$) is charge transferred calculated with calibration curve.
[d] ±values are the standard errors derived from duplicate sample injections.

Table S8. Comparison of EDC and EAC between values obtained by direct calculation using Faraday constant and calibration curve using redox standard in MCA analysis for pyDOM and NOM samples.

Sample	EDC by calibration ($mmol_{e-}\cdot g_C^{-1}$) [a]	EDC by direct calculation ($mmol_{e-}\cdot g_C^{-1}$) [a,b]	Difference	EAC by calibration ($mmol_{e-}\cdot g_C^{-1}$) [a]	EAC by direct calculation ($mmol_{e-}\cdot g_C^{-1}$) [a,b]	Difference
$pyDOM_{W300}$	0.34±0.08	0.35±0.08	3%	1.68±0.10	1.74±0.10	4%
$pyDOM_{W400}$	0.54±0.13	0.56±0.13	3%	2.61±0.63	2.71±0.67	4%
$pyDOM_{W500}$	0.70±0.09	0.71±0.10	3%	5.52±0.42	5.75±0.44	4%
$pyDOM_{W600}$	0.17±0.05	0.16±0.05	2%	4.21±0.35	4.38±0.37	4%
$pyDOM_{W700}$	0.29±0.04	0.28±0.04	3%	1.46±0.05	1.48±0.05	1%
$pyDOM_{G300}$	0.46±0.12	0.47±0.12	4%	1.58±0.23	1.64±0.24	4%
$pyDOM_{G400}$	0.73±0.01	0.74±0.01	3%	2.75±0.14	2.82±0.15	3%
$pyDOM_{G500}$	0.33±0.08	0.32±0.09	2%	4.70±0.20	4.88±0.21	3%
$pyDOM_{G600}$	0.31±0.05	0.30±0.05	2%	4.93±0.36	5.11±0.38	4%
$pyDOM_{G700}$	0.18±0.05	0.18±0.06	3%	1.63±0.07	1.70±0.07	4%
ESHA	1.04±0.13	1.08±0.13	3%	2.11±0.45	2.21±0.48	5%
LHA	2.41±0.02	2.50±0.02	3%	3.51±0.65	3.68±0.68	5%
PPFA	2.06±0.12	2.14±0.13	4%	1.32±0.16	1.39±0.17	5%
PPHA	1.69±0.40	1.75±0.41	4%	2.06±0.02	2.17±0.02	5%
SRFA	4.84±0.05	5.03±0.06	4%	0.72±0.00	0.76±0.00	5%
SRNOM	2.56±0.02	2.66±0.02	4%	1.08±0.12	1.14±0.12	5%

[a] ±values are the standard errors derived from duplicate sample injections.
[b] Values were calculated using the peak area (PA) (**Table S7**) divided by the injected non-purgeable organic carbon (NPOC) and Faraday constant ($F = 96{,}485\ s\cdot A\cdot mol_{e-}^{-1}$).

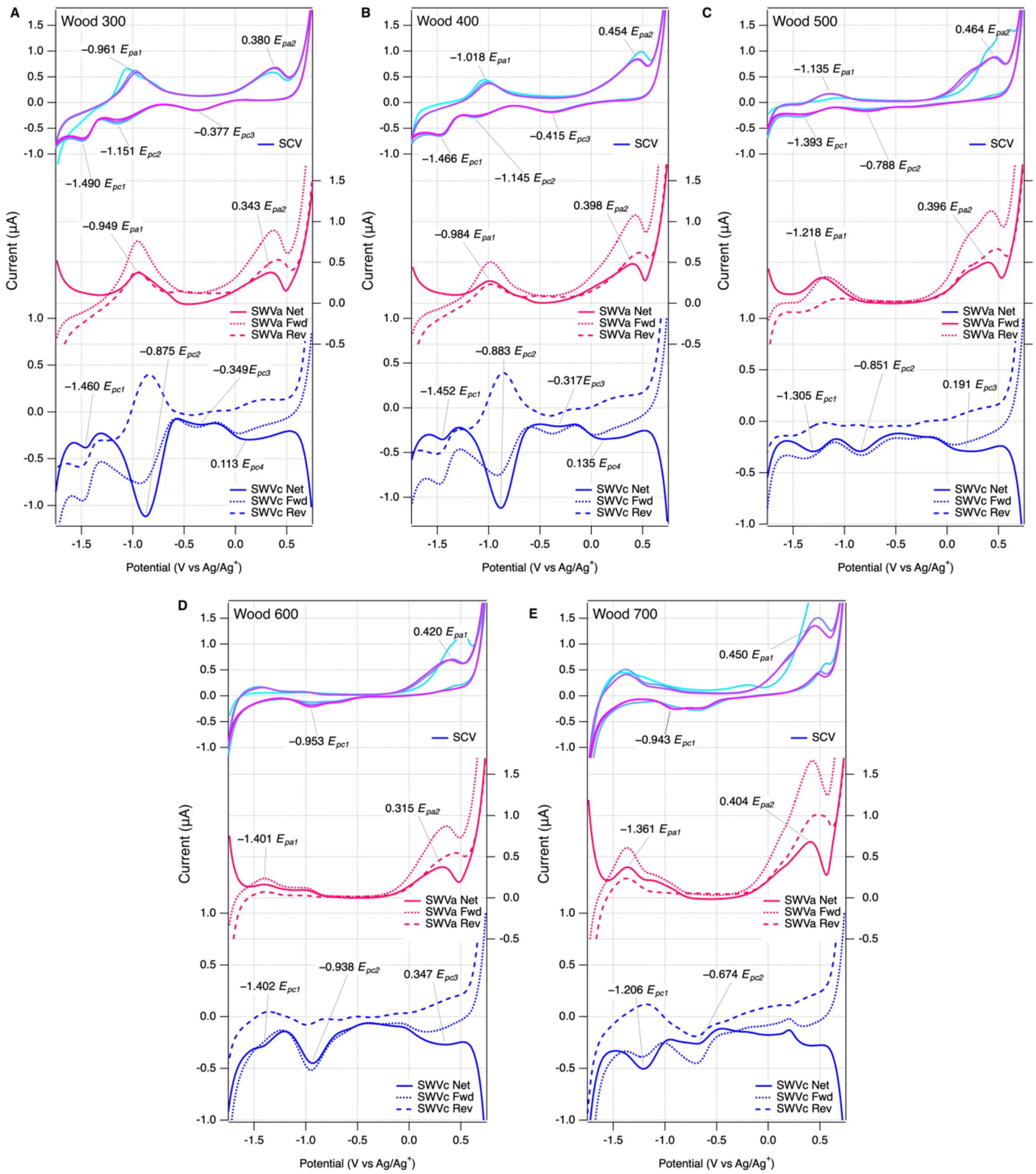

Figure S3. SCV (top), SWVa (middle), SWVc (bottom) of pyDOM derived from Wood 300 to 700 (panel A to E). SCV (3 scans) color change is denoted by passage of time (lightest to darkest). SWV components include forward, reverse and net current. All data is background subtracted. Experiments performed in 0.1 M TBAFP in DMSO (5 mL DMSO and 0.5 mL spike of analyte in phosphate buffer at pH 7). Pt working electrode, Ag/Ag^{+} reference electrode, and Pt wire counter electrode were used for analysis. PyDOM concentrations varied and are normalized to NPOC. Scan rate was 25 mV s^{-1}, step size was 2 mV, and amplitude was 25 mV (SWV).

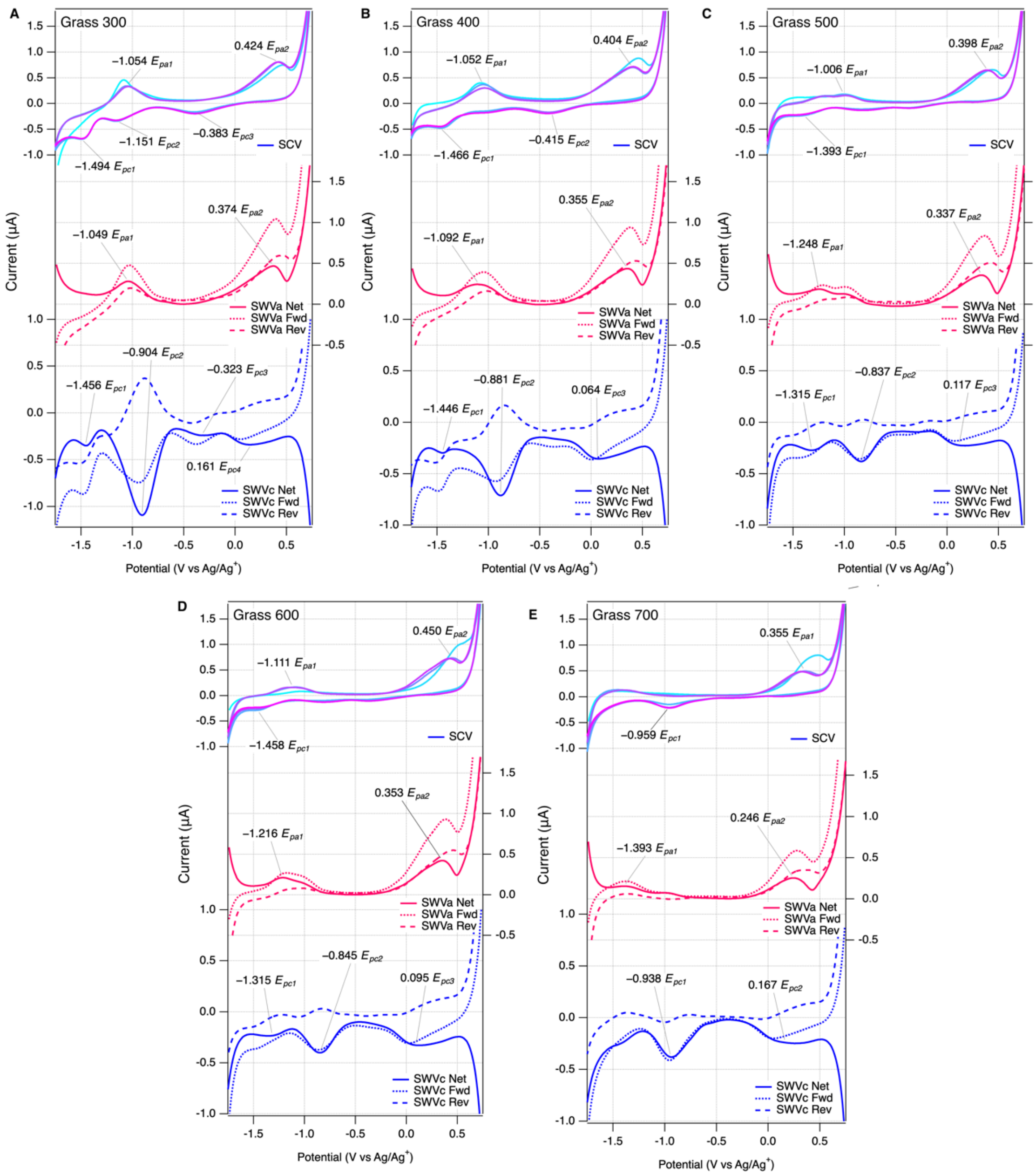

Figure S4. SCV (top), SWVa (middle), SWVc (bottom) of pyDOM derived from Grass 300 to 700 (panel A to E). SCV (3 scans) color change is denoted by passage of time (lightest to darkest). SWV components include forward, reverse and net current. All data is background subtracted. Experiments performed in 0.1 M TBAFP in DMSO (5 mL DMSO and 0.5 mL spike of analyte in phosphate buffer at pH 7). Pt working electrode, Ag/Ag^+ reference electrode, and Pt wire counter electrode were used for analysis. PyDOM concentrations varied and are normalized to NPOC. Scan rate was 25 mV s^{-1}, step size was 2 mV, and amplitude was 25 mV (SWV).

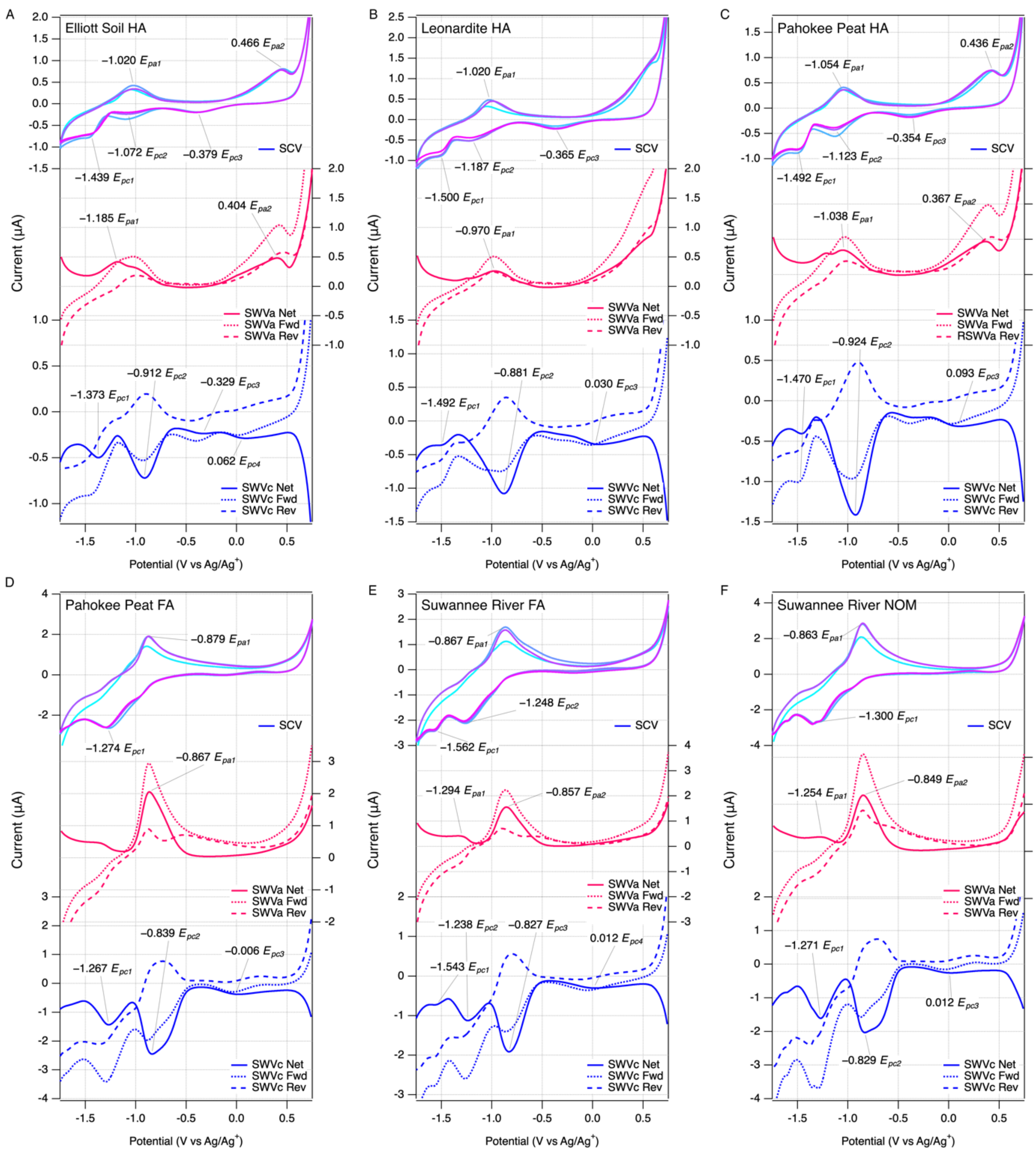

Figure S5. SCV (top), SWVa (middle), SWVc (bottom) of NOMs. SCV (3 scans) color change is denoted by passage of time (lightest to darkest). SWV components include forward, reverse and net current. All data is background subtracted. Experiments performed in 0.1 M TBAFP in DMSO (5 mL DMSO and 0.5 mL spike of analyte in phosphate buffer at pH 7). Pt working electrode, Ag/Ag^+ reference electrode, and Pt wire counter electrode were used for analysis. Scan rate was 25 mV s^{-1}, step size was 2 mV, and amplitude was 25 mV (SWV).

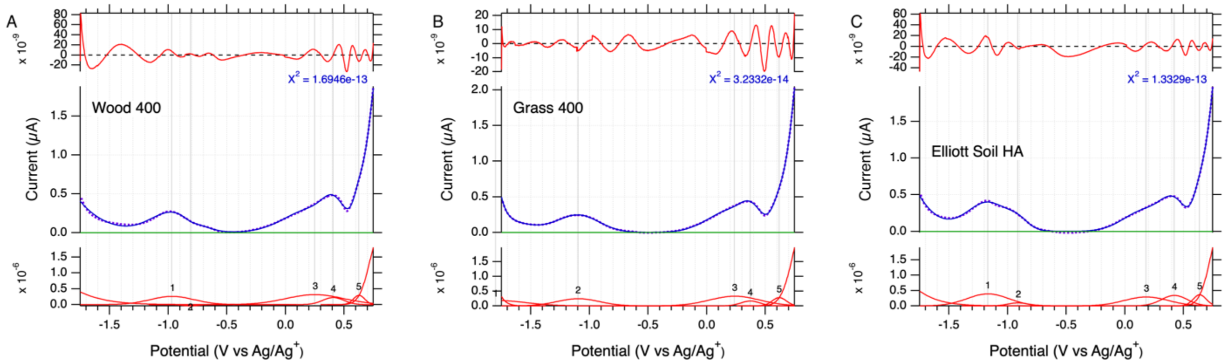

Figure S6. Representative pyDOM and NOM multipeak fit results for SWVa net current using Igor v9. The middle blue solid line is the net current response, the purple dotted line on top denotes the fit, the green line is the constant baseline (y = 0). The red lines at the top are the residuals and the chi-square statistic is listed underneath (right) in purple. The bottom red lines show the individual fitted gaussian peaks. All data is background subtracted.

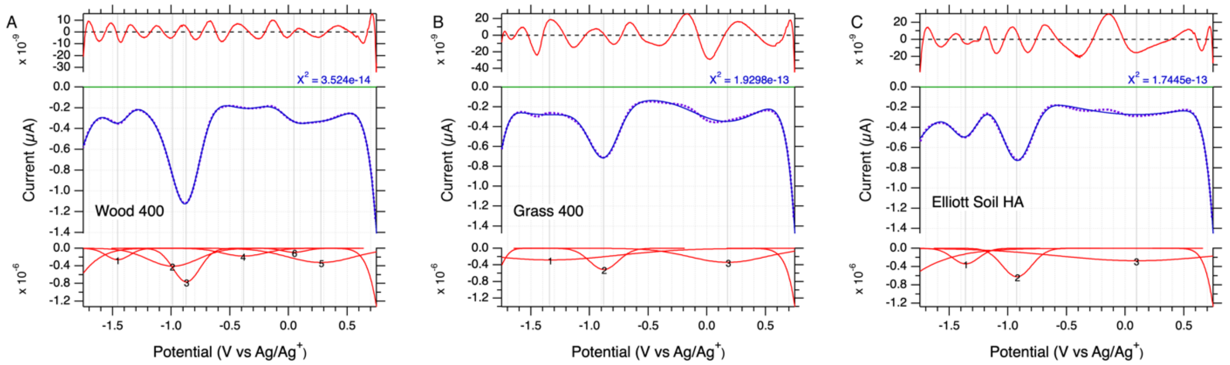

Figure S7. Representative pyDOM and NOM multipeak fit results for SWVc net current using Igor v9. The middle blue solid line is the net current response, the purple dotted line on top denotes the fit, the green line is the constant baseline (y = 0). The red lines at the top are the residuals and the chi-square statistic is listed underneath (right) in purple. The bottom red lines show the individual fitted gaussian peaks. All data is background subtracted.

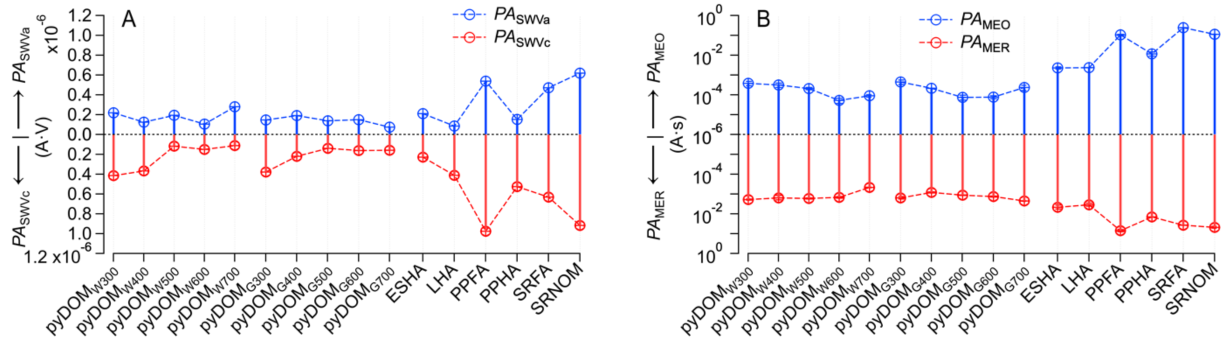

Figure S8. (A) Anodic peak area (PA_{SWVa}) and cathodic peak area (PA_{SWVc}) measured by square-wave voltammetry (SWV), and (B) oxidative peak area (PA_{MEO}) and reductive peak area (PA_{MER}) measured by mediated chronoamperometry (MCA). The error bars of MCA values were derived from duplicate injections of each sample. The lines and symbols in blue represent PA_{SWVa} and PA_{MEO}, while the ones in red represent PA_{SWVc} and PA_{MER}, respectively. The pyDOM were derived from wood (*Quercus*) and grass (*Panicum vigartum*) biomass at different temperatures (300 to 700 °C), which were denoted as $pyDOM_{WX}$ and $pyDOM_{GX}$, respectively. The W and G represents wood or grass feedstock, respectively, whereas X corresponds to the pyrolysis temperature. Abbreviations for NOMs are given in **Table S1**.

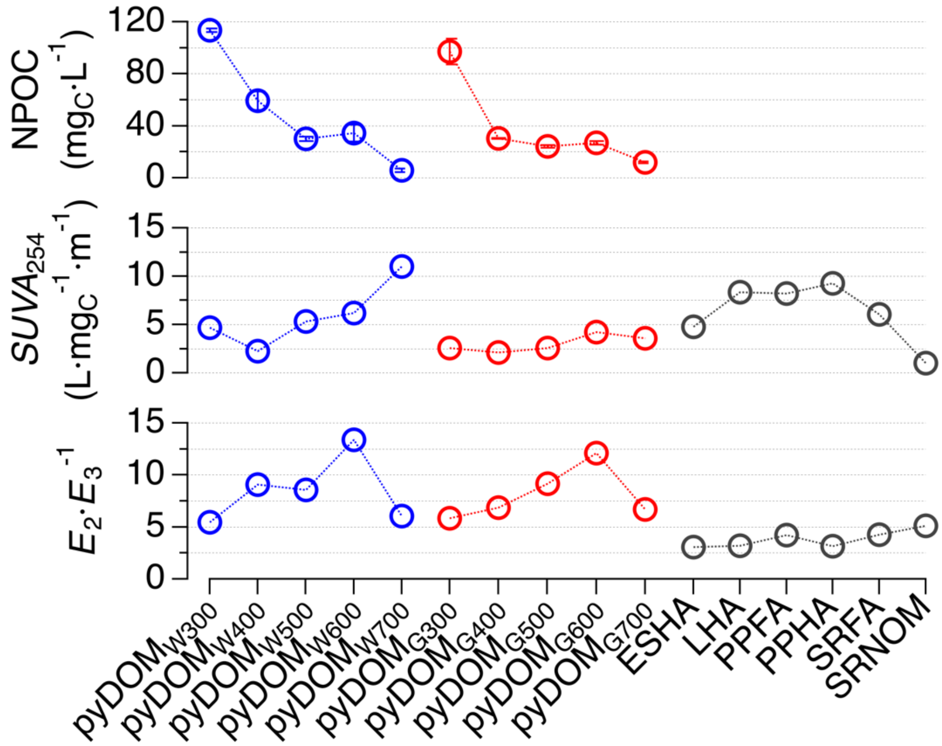

Figure S9. Non-purgeable organic carbon (NPOC), the specific UV absorbance at 254 nm ($SUVA_{254}$) values and $E_2 \cdot E_3^{-1}$ ratios (top, middle and bottom, respectively) of pyDOM and NOM samples.The NPOC of pyDOM were extracted from respective chars at 20 $g_{char} \cdot L^{-1}$. The error bars of NPOC were based on duplicate measurements of individually prepared samples. The pyDOM were derived from wood (*Quercus*) and grass (*Panicum vigartum*) biomass pyrolyzed at different temperatures (300 to 700 °C), which were denoted as $pyDOM_{WX}$ and $pyDOM_{GX}$, respectively. The W or G represents wood or grass feedstock, respectively, followed by the pyrolysis temperature. Abbreviations for NOMs are given with **Table S1**.

Text S4. Correlation analysis of EECs vs. $SUVA_{254}$, $E_2 \cdot E_3^{-1}$, iron (Fe), manganese (Mn), H/C ratio, and O/C ratio.

Correlation analysis of the EEC data vs. independently measured properties of the samples might provide explanatory (or predictive) relationships. To this end, we plot EECs by both SWV and MCA vs. $SUVA_{254}$ and $E_2 \cdot E_3^{-1}$ (from **Table S3**), iron (Fe) and manganese (Mn) content (from **Table S4**), and H/C and O/C ratio (from **Tables S1 and S2**) in **Figure S10**. Neither MCA nor SWV values correlate well to the independent factors from panels A to F , although the $SUVA_{254}$ and $E_2 \cdot E_3^{-1}$ are typical indicators of aromaticity and molecular size for dissolved organic species,[5,6] while Fe and Mn are common redox metals present in NOM that can affect the redox activity of NOM samples. We took similar approach as our previous study[7] to calculate metal contributions to the EEC_{MCA} of pyDOM (**Table S4**). Similar results as our previous study were observed, which showed the contribution of Fe is negligible, but Mn be more significant (assuming the Mn^{4+}/Mn^{2+} redox pair undergoes 2 mole e^- per mole Mn). Nonetheless, the individual contribution of the metals should be evaluated with caution, since the valence states of the metals were unknown.

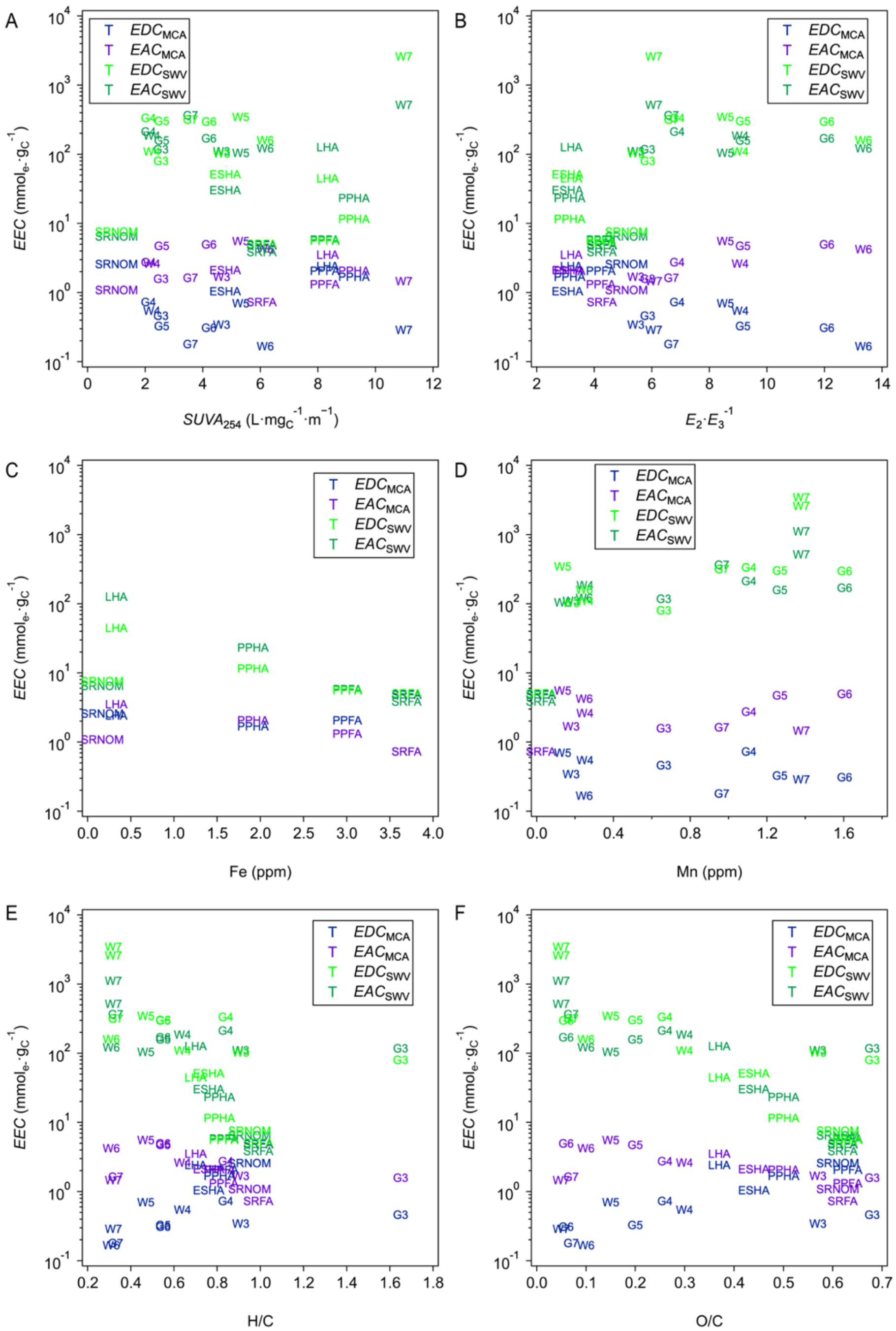

Figure S10. Correlations of EEC derived from SWV and MCA versus various independent factors of NOM and pyDOM, including (A) $SUVA_{254}$, (B) $E_2 \cdot E_3^{-1}$, (C) Fe, (D) Mn, (E) H/C ratio, and (F) O/C ratio. The $SUVA_{254}$ and $E_2 \cdot E_3^{-1}$ values were adopted from NOM and pyDOM in **Table S3**. The Fe and Mn contents were adopted from NOM and pyDOM in **Table S4**. The H/C and O/C ratios were adopted from NOM in **Tables S1,** and from char in **Table S2**. The labels in cyan and green represent SWV values, while those in blue and purple represent MCA values.

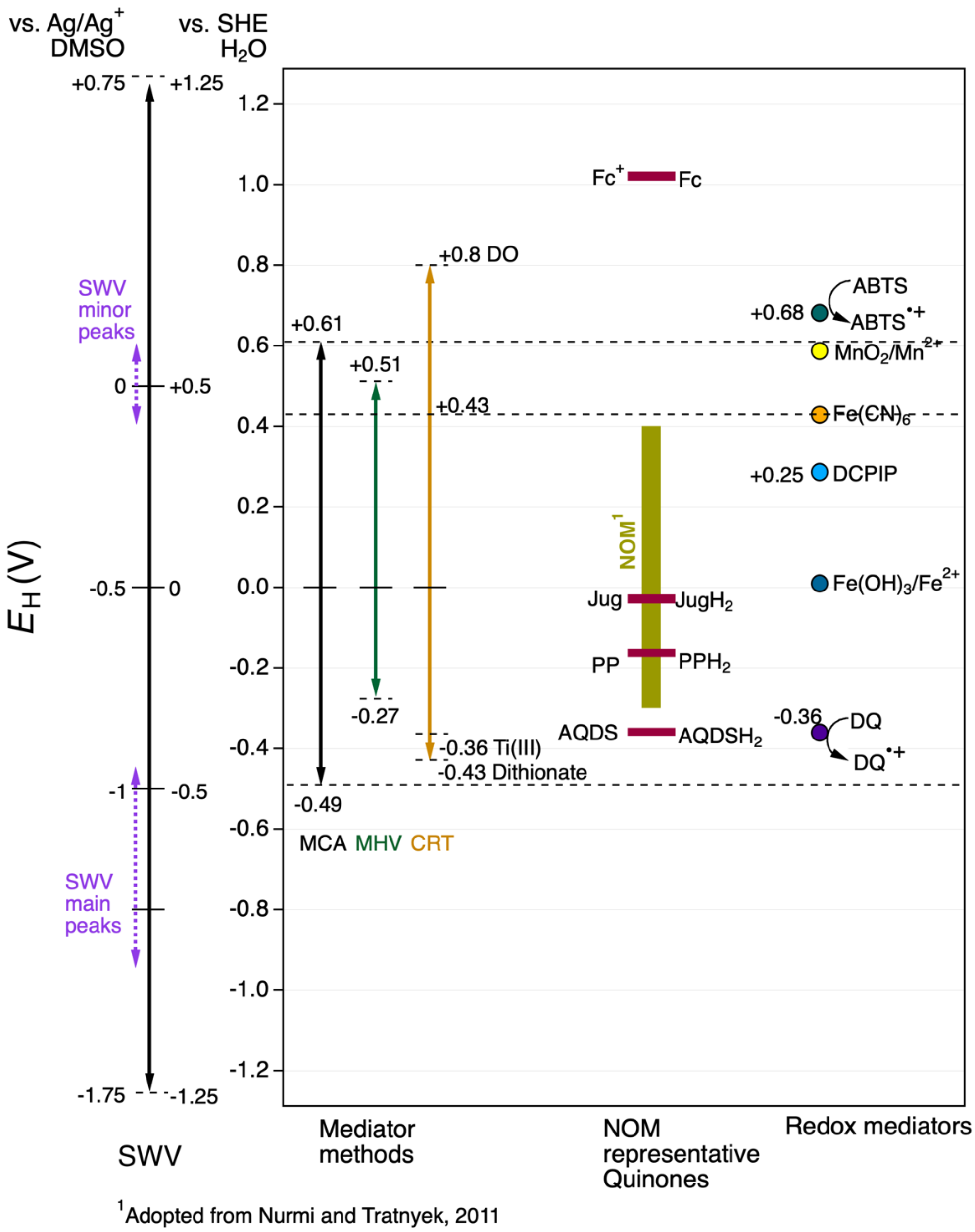

Figure S11. Redox ladder of redox potential ranges from different studies of mediator methods, including mediated chronoamperometry (MCA), mediated hydrodynamic voltammetry (MHV) and chemical redox titration (CRT). The redox potential range of NOM representative quinones were adopted from other studies.[8,9] The NR in MHV method represents neutral red, while the DO in CRT method represents dissolved oxygen. The reduction potentials of common redox couples are listed for reference purpose. The entire potential range covers the applied SWV sweeping potential, which ranges from −1.75 V vs. Ag/Ag^+ in DMSO (−1.25 V vs. standard electron potential (SHE)) to +0.75 V vs. Ag/Ag^+ in DMSO (+1.25 V vs. SHE).

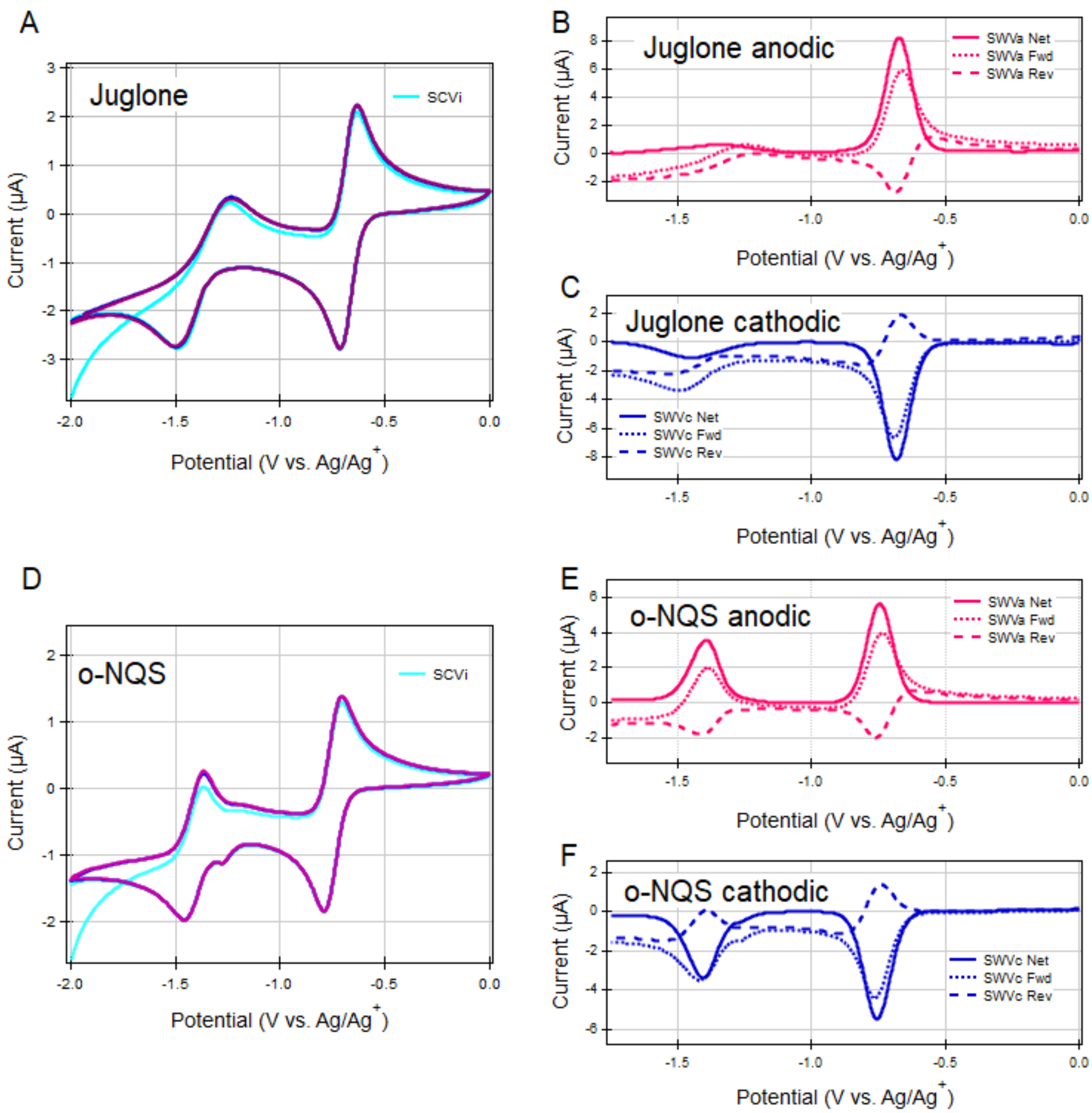

Figure S12. SCV of (A) juglone and (D) o-NQS, along with representative anodic and cathodic SWV voltammograms of juglone (B and C) and o-NQS (E and F). Color schemes and annotations are defined in **Figures S3-S5**.

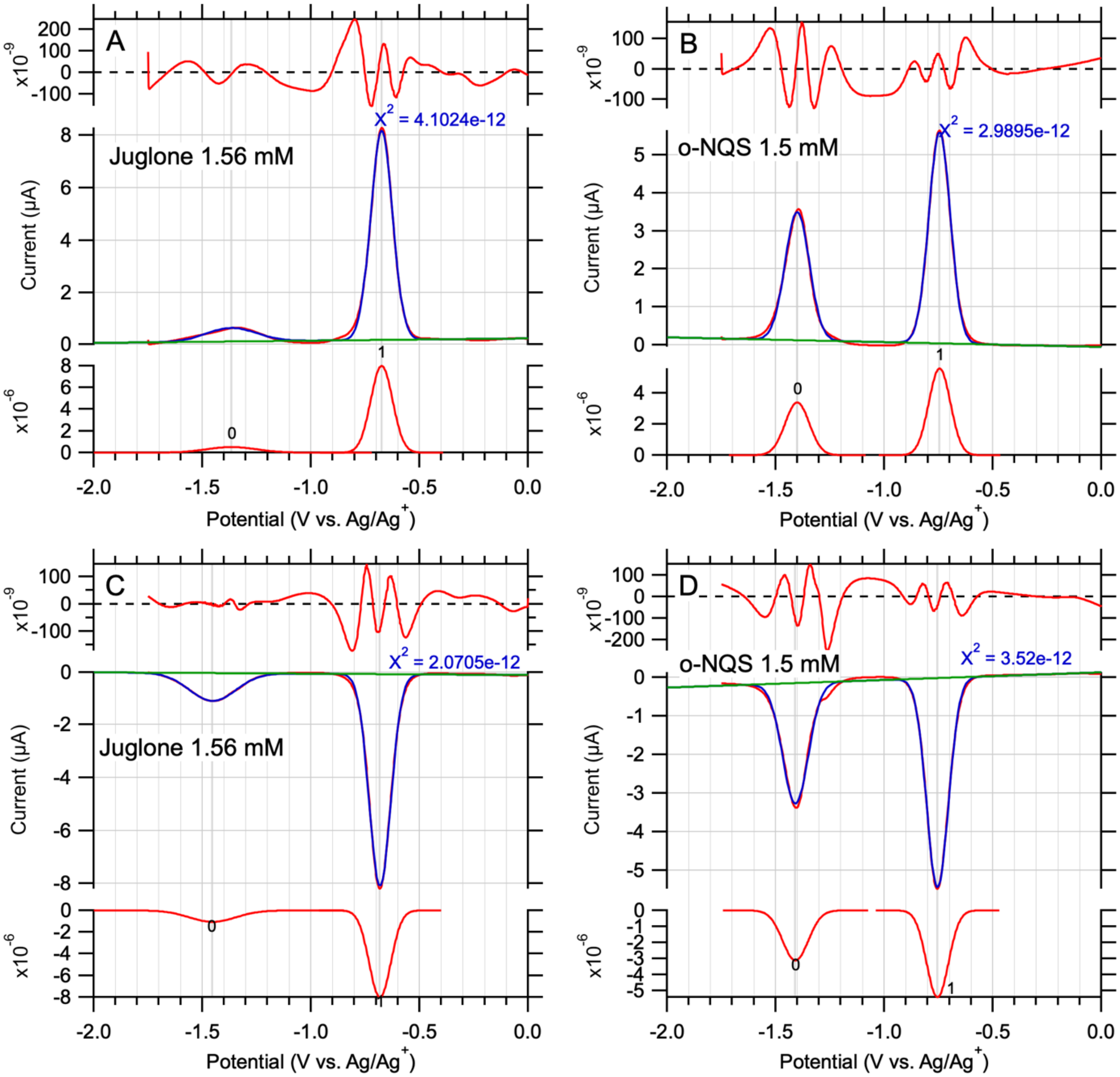

Figure S13. Fitting analysis of SWVa peak responses (A and B) and SWVc peak responses (C and D) in experiments with juglone (A and C) and o-NQS (B and D) performed in Igor Pro. Arrangement of figure parts is defined in **Figures S6 and S7**.

Table S9. Method validation of SWV using RS (model quinones).

Model Quinone	PA_{SWVa} [a]	PA_{SWVc} [a]	EDC_{SWV} ($mmol_{e-}\cdot mmol_{RS}^{-1}$)	EAC_{SWV} ($mmol_{e-}\cdot mmol_{RS}^{-1}$)
Juglone	1.00E−06	9.97E−07	3.15E+00	1.86E+00
o-NQS	6.93E−07	6.81E−07	2.29E+00	1.35E+00

[a] PA is peak area (inner area only, excluding one outermost peak on each side) (A·V).

Table S10. Method validation of MCA using RS (model quinones).

Model Quinone	NPOC ($mg_C\cdot L^{-1}$) [a]	EDC_{MCA} ($mmol_{e-}\cdot g_C^{-1}$) [a]	EAC_{MCA} ($mmol_{e-}\ g_C^{-1}$) [a]	EDC_{MCA} ($mmol_{e-}\cdot mmol_{RS}^{-1}$) [a]	EAC_{MCA} ($mmol_{e-}\cdot mmol_{RS}^{-1}$) [a]
Juglone	47.2±0.38	0.46±0.01	19.41±1.83	0.06±0.00	2.34±0.00
o-NQS	514.0±2.40	0.24±0.00	16.55±1.23	0.03±0.00	1.99±0.15

[a] ±values are the standard errors from duplicate injections of each sample.

Text S5. Unit conversion for EECs of char.

All EECs of char that we adopted from previous studies were reported in the unit of $mmol_{e-}\cdot g_{char}^{-1}$, while those of pyDOM were reported in the unit of $mmol_{e-}\cdot g_{C}^{-1}$. Therefore, extra steps were carried out in reconciling the units so that direct comparison of EECs could be made between char and pyDOM. In **Figure 5**, units of all char EECs were converted to $mmol_{e-}\cdot g_{C}^{-1}$ by dividing the reported weight percentage (wt%) of carbon from their corresponding elemental analyses. Some of these studies reported the carbon content in the unit of $mmol_{C}\cdot g_{char}^{-1}$,[10,11] while other studies directly reported the weight percentage (wt%) of carbon.[1,12-17] For the former studies, wt% of carbon was calculated by multiplying the molecular weight of carbon (i.e. 12 $mg_{C}\cdot mmol_{C}^{-1}$) with eq S8 before unit conversion.

$$\textbf{wt\% of carbon} = \frac{\textbf{carbon content } (\mathbf{mmol_{C}\cdot g_{char}^{-1}})\cdot \mathbf{M_w}}{\mathbf{1000}} \tag{S8}$$

where wt% represents weight percentage ($g_{C}\cdot g_{char}^{-1}$), and M_w represents molecular weight of carbon (i.e., 12 $mg_{C}\cdot mmol_{C}^{-1}$).

Then, all reported EEC values of char were divided by their respective wt% of carbon to obtain the values after conversion, showed in eq S9.

$$\textbf{EECs of char } (\mathbf{mmol_{e-}\cdot g_{C}^{-1}}) = \frac{\textbf{EECs of char } (\mathbf{mmol_{e-}\cdot g_{char}^{-1}})}{\textbf{wt\% of carbon}} \tag{S9}$$

Table S11. The EDC and EAC values of char and pyDOM adopted from literatures for compiling **Figure 5**.

Source material	Pyrolysis T (°C)	EDC [a] ($mmol_{e-}\cdot gC^{-1}$)	EAC [a] ($mmol_{e-}\cdot gC^{-1}$)	EEC [a] ($mmol_{e-}\cdot gC^{-1}$)	Method [b]	Potential used/range (vs. SHE)	pH	Mediator/redox species	Ref
Pine wood (char)	400	8.95	0.26	9.21	MHV	+0.51 V −0.27 V	6.5	Fe (III)/Fe (II) NR_{RED}/NR	[10]
	500	4.42	0.48	4.9					
	600	1.55	0.11	1.66					
Soil reef (char)	550	2.70	3.37	6.07	CRT	+0.43 V −0.36 V	7 (EDC) 6.4 (EAC)	Fe (III)/Fe (II) Ti(III)/Ti (IV) Dithionite	[12]
Walnut (char)	400	0.00026	0.00026	0.00052	CV	1.5 V	7	N/A	[1]
	450	0.00029	0.00029	0.00058					
	500	0.00049	0.00049	0.00098					
	550	0.00052	0.00052	0.00104					
	600	0.00022	0.00022	0.00044					
	650	2.25E-05	2.25E-05	0.000045					
Pine wood (char)	200	0.29	0.0098	0.2998	MCA	+0.61 V −0.49 V	7	$ABTS^{\bullet+}$/ABTS $ZiV^{\bullet-}$/ZiV	[11]
	300	0.37	0.037	0.407					
	400	0.27	0.35	0.62					
	500	0.037	0.66	0.697					
	600	0.034	0.169	0.203					
	700	0.033	0.24	0.273					
Switch grass (char)	200	0.25	0.04	0.29					
	300	0.57	0.10	0.67					
	400	0.91	1.16	2.07					
	500	0.29	0.97	1.26					
	600	0.11	0.69	0.8					
	700	0.12	0.80	0.92					

Hazel nut (char)	400	0.28	1.26	1.54					
	550	0.16	0.46	0.62					
	700	0.14	0.40	0.54					
Douglas fir (char)	400	0.062	0.45	0.512					
	700	0.20	0.57	0.77					
Rice straw (char)	450	0.69	1.51	2.2					
Chestnut (char)	450	0.53	1.88	2.41					
Olive tree (char)	400	0.30	0.21	0.51	MCA	+0.61 V −0.28 V	7	$ABTS^{\bullet+}/ABTS$ Neutral Red	13
	600	0.19	0.25	0.44					
	800	0.05	0.091	0.141					
	1000	0.039	0.039	0.078					
Almond tree (char)	400	0.31	0.12	0.43					
Orange tree (char)	400	0.37	0.61	0.98					
Rice straw (char)	250	0.063	0.047	0.11	MCA	+0.61 V −0.49 V	7	$ABTS^{\bullet+}/ABTS$ $ZiV^{\bullet-}/ZiV$	14
	350	0.054	0.054	0.108					
	450	0.037	0.098	0.135					
	550	0.012	0.12	0.132					
	650	0.024	0.12	0.144					
	750	0.012	0.093	0.105					
	850	0.011	0.080	0.091					
	950	0.011	0.057	0.068					
Cellulose (char)	300	0.20	0.045	0.245	MCA	+0.61 V −0.49 V	7	$ABTS^{\bullet+}/ABTS$ $DQ^{\bullet+}/DQ^{2+}$	15
	500	0.14	0.21	0.35					

	700	0.1	0.3	0.4					
Lignin (char)	300	0.35	0.015	0.365					
	500	0.54	0.38	0.92					
	700	0.43	0.85	1.28					
Barley grass (char)	200	2.70	0.46	3.16	MCA	+0.61 V −0.49 V	7	$ABTS^{\bullet+}/ABTS$ $ZiV^{\bullet-}/ZiV$	[16]
	350	2.70	0.66	3.36					
	400	1.27	0.83	2.1					
	450	1.09	0.66	1.75					
	500	0.37	0.68	1.05					
	650	0.61	0.80	1.41					
	700	0.35	0.68	1.03					
	800	0.83	1.09	1.92					
Pine wood (pyDOM)	200	6.54	0.45	6.99	FIA	+0.70 V −0.41 V	7	$ABTS^{\bullet+}/ABTS$ $ZiV^{\bullet-}/ZiV$	[7]
	300	2.92	0.28	3.2					
	400	1.46	0.31	1.77					
	500	0.74	0.50	1.24					
	600	2.01	1.19	3.2					
	700	0.34	0.24	0.58					
Switch grass (pyDOM)	200	1.53	0.16	1.69					
	300	2.86	0.24	3.1					
	400	2.40	0.62	3.02					
	500	0.97	0.46	1.43					
	600	0.33	0	0.33					
	700	0.40	0	0.4					
Rice straw (pyDOM)	450	2.01	0.62	2.63					
Chestnut (pyDOM)	450	2.3	0.53	2.83					

Soybean (pyDOM)	400	3.38	0.4	3.78	MCA	+0.61 V −0.49 V	7	$ABTS^{\bullet+}/ABTS$ $DQ^{\bullet+}/DQ^{2+}$	18
Wheat (pyDOM)		2.42	0.41	2.83					
Rice (pyDOM)		7.1	0.8	7.9					
Sorghum (pyDOM)		4.2	1.3	5.5					
Peanut (pyDOM)		5.51	0.7	6.21					
Corn (pyDOM)		3.24	0.81	4.05					
Wheat straw (pyDOM)	300 400 500 600 700	0.05 0.1 0.14 0.06 0.02	0.01 0.19 0.31 0.12 0.05	0.06 0.29 0.45 0.18 0.07	MCA	+0.61 V −0.49 V	7	$ABTS^{\bullet+}/ABTS$ $DQ^{\bullet+}/DQ^{2+}$	19

[a] Some of the values differ from origincated study due to the unit difference, which the conversion of unit was provided in **Text S5**.

[b] MHV refers to mediated hydrodynamic voltammetry, CRT refers to chemical redox titration, CV refers to cyclic voltammetry, MCA refers to mediated chronoamperometry, and FIA refers to flow-injection analysis.

References

1. T. Sun, B. D. A. Levin, J. J. L. Guzman, A. Enders, D. A. Muller, L. T. Angenent and J. Lehmann, Rapid electron transfer by the carbon matrix in natural pyrogenic carbon, *Nature Communications*, 2017, **8**, 14873, 10.1038/ncomms14873
2. N. Walpen, G. J. Getzinger, M. H. Schroth and M. Sander, Electron-donating phenolic and electron-accepting quinone moieties in peat dissolved organic matter: quantities and redox transformations in the context of peat biogeochemistry, *Environmental Science & Technology*, 2018, **52**, 5236-5245, 10.1021/acs.est.8b00594
3. H. Wang, R. Emanuelsson, A. Banerjee, R. Ahuja, M. Strømme and M. Sjödin, Effect of cycling ion and solvent on the redox chemistry of substituted quinones and solvent-induced breakdown of the correlation between redox potential and electron-withdrawing power of substituents, *The Journal of Physical Chemistry C*, 2020, **124**, 13609-13617, doi.org/10.1021/acs.jpcc.0c03632
4. M. Quan, D. Sanchez, M. F. Wasylkiw and D. K. Smith, Voltammetry of quinones in unbuffered aqueous solution: reassessing the roles of proton transfer and hydrogen bonding in the aqueous electrochemistry of quinones, *Journal of the American Chemical Society*, 2007, **129**, 12847-12856, doi.org/10.1021/ja0743083
5. T. Jamieson, E. Sager and C. Guéguen, Characterization of biochar-derived dissolved organic matter using UV–visible absorption and excitation–emission fluorescence spectroscopies, *Chemosphere*, 2014, **103**, 197-204, doi.org/10.1016/j.chemosphere.2013.11.066
6. J. T. Nurmi and P. G. Tratnyek, Electrochemical properties of natural organic matter (NOM), fractions of NOM, and model biogeochemical electron shuttles, *Environmental Science & Technology*, 2002, **36**, 617-624, 10.1021/es0110731
7. W. Xu, N. Walpen, M. Keiluweit, M. Kleber and M. Sander, Redox Properties of Pyrogenic Dissolved Organic Matter (pyDOM) from Biomass-Derived Chars, *Environmental Science & Technology*, 2021, **55**, 11434-11444, 10.1021/acs.est.1c02429
8. J. T. Nurmi and P. G. Tratnyek, Electrochemistry of Natural Organic Matter in *Aquatic Redox Chemistry*, eds. P. G. Tratnyek, T. J. Grundl and S. B. Haderlein, American Chemical Society, Washington, DC, 2011, vol. 1071, ch. 7, pp. 129-151.
9. M. Aeschbacher, M. Sander and R. P. Schwarzenbach, Novel electrochemical approach to assess the redox properties of humic substances, *Environmental Science & Technology*, 2010, **44**, 87-93, doi.org/10.1021/es902627p
10. A. Prévoteau, F. Ronsse, I. Cid, P. Boeckx and K. Rabaey, The electron donating capacity of biochar is dramatically underestimated, *Scientific reports*, 2016, **6**, 32870, 10.1038/srep32870
11. L. Klüpfel, M. Keiluweit, M. Kleber and M. Sander, Redox properties of plant biomass-derived black carbon (biochar), *Environmental Science & Technology*, 2014, **48**, 5601-5611, 10.1021/es500906d
12. D. Xin, M. Xian and P. C. Chiu, New methods for assessing electron storage capacity and redox reversibility of biochar, *Chemosphere*, 2019, **215**, 827-834, doi.org/10.1016/j.chemosphere.2018.10.080
13. F. J. Chacón, M. A. Sánchez-Monedero, L. Lezama and M. L. Cayuela, Enhancing biochar redox properties through feedstock selection, metal preloading and post-pyrolysis treatments, *Chemical Engineering Journal*, 2020, **395**, 125100, doi.org/10.1016/j.cej.2020.125100

14. H. Wang, H.-P. Zhao and L. Zhu, Role of pyrogenic carbon in parallel microbial reduction of nitrobenzene in the liquid and sorbed phases, *Environmental Science & Technology*, 2020, **54**, 8760-8769, 10.1021/acs.est.0c01061
15. S. Li, L. Shao, H. Zhang, P. He and F. Lü, Quantifying the contributions of surface area and redox-active moieties to electron exchange capacities of biochar, *Journal of Hazardous Materials*, 2020, **394**, 122541, doi.org/10.1016/j.jhazmat.2020.122541
16. Y. Zhang, X. Xu, L. Cao, Y. S. Ok and X. Cao, Characterization and quantification of electron donating capacity and its structure dependence in biochar derived from three waste biomasses, *Chemosphere*, 2018, **211**, 1073-1081, doi.org/10.1016/j.chemosphere.2018.08.033
17. Y. Zhang, X. Xu, P. Zhang, Z. Ling, H. Qiu and X. Cao, Pyrolysis-temperature depended quinone and carbonyl groups as the electron accepting sites in barley grass derived biochar, *Chemosphere*, 2019, **232**, 273-280, doi.org/10.1016/j.chemosphere.2019.05.225
18. X. Zheng, Y. Liu, H. Fu, X. Qu, M. Yan, S. Zhang and D. Zhu, Comparing electron donating/accepting capacities (EDC/EAC) between crop residue-derived dissolved black carbon and standard humic substances, *Science of The Total Environment*, 2019, **673**, 29-35, doi.org/10.1016/j.scitotenv.2019.04.022
19. B. Zhang, S. Zhou, L. Zhou, J. Wen and Y. Yuan, Pyrolysis temperature-dependent electron transfer capacities of dissolved organic matters derived from wheat straw biochar, *Science of The Total Environment*, 2019, **696**, 133895, doi.org/10.1016/j.scitotenv.2019.133895